# Feedback Parameter Selection for Impedance Control of Series Elastic Actuators

Ye Zhao, Nicholas Paine and Luis Sentis

***Abstract*—The interest of series elastic actuators (SEAs) for legged robots has recently increased to achieve compliant interactions and efficient gaits. However, control of legged robots with SEAs is difficult due to the need to design controllers that take into account both torque and impedance feedback loops. The work presented here addresses this issue by proposing a critically-damped fourth order system gain selection criterion for a cascaded SEA control structure with inner torque and outer impedance feedback loops. Velocity filtering and feedback delays are taken into consideration for stability and impedance performance analysis. We observe and analyze the interdependence between torque and impedance feedback gains to achieve the desired closed loop performance. Based on this analysis we derive a simple gain design criterion to maximize the tracking performance of SEAs. Our final goal is to maximize the output impedance capabilities of SEAs in order to fulfill a wide range of application needs. In contrast to low impedance design studies, we focus here specifically on achieving the highest possible impedance gains of SEAs. Finally, experiments using our UT-SEA are conducted to verify our proposed approach. This study serves as a stepping stone towards utilizing and designing humanoid robots with SEA actuators for mobile behaviors and interaction with cluttered and unknown environments.**

## I. Introduction

Cascaded control structures for series elastic actuators (SEAs) [1] have gained attention during the past decade [2], [3], [4]. This type of structure utilizes multiple nested control loops to achieve robustness and disturbance rejection. Existing studies proposed one type of cascaded structure with an inner torque loop for controlling SEA dynamics and an outer impedance loop for modulating high-level tasks [5], [3]. More recently, investigations have been made to add an inner-most motor velocity feedback loop nested inside the torque loop [2], [3], [4]. This velocity loop enables the motor to behave as a velocity source, eliminating the need to model drivetrain friction. The results in [5] analyzed various cascaded loops including torque, velocity and position feedback loops.

Impedance control is suitable for dynamic interaction control between a robot and its environment [6]. In general, control designers often choose low impedance as a design target of SEAs for compliant performance [3], [4]. However, different tasks require different impedances and high impedance for SEAs will benefit "stiff" tasks. For instance, without feedforward compensation, legged robots require high stiffness to counteract the effects of gravity. Our target is to maximize the impedance range of series elastic actuator, i.e., the Z-width [7], [8]. Since low or near-zero impedance has already been explored successfully [9], [1], we focus more on the achievable high impedance of SEAs, which is rarely explored to the authors' best knowledge. It should be kept in mind that the impedance of SEAs still can not reach as high as that of rigid actuators. In fact, SEA impedance is limited by the user-defined virtual stiffness at low frequencies and by spring stiffness at high frequencies [3].

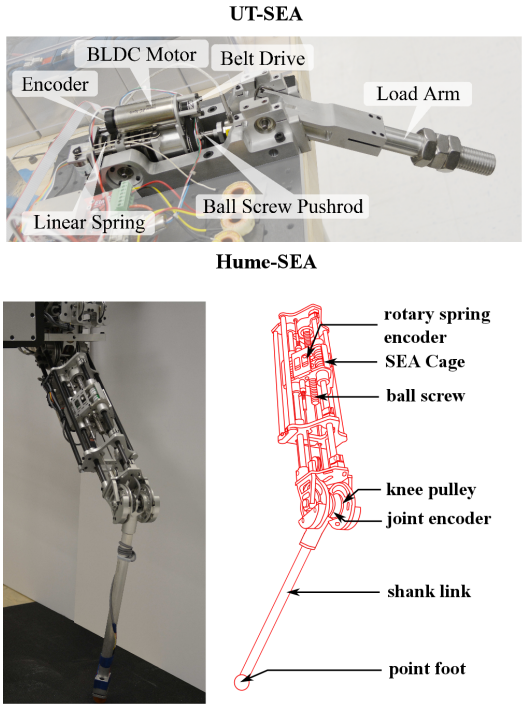


Fig. 1. **UT-SEA and Hume-SEA.** This figure shows two types of series elastic actuators. The upper one is the high-performance UT-SEA test bed. The lower one is our Hume bipedal robot with series elastic actuators.

Series elastic actuators have high-order system dynamics. Designing controller gains for their several cascaded loops is challenging and there is still a lack of convincing methodologies for this type of control design. Most existing results rely on empirical tuning [1], [5]. In [3], the authors use a passivity criterion to derive controller gain ranges. However, these ranges are inequalities and gain parameters are coupled together, which makes controller gain selection still complex. Recently, we proposed a critically-damped gain selection criterion to achieve high impedance for rigid actuators while incorporating effects from signal filtering and feedback delays [10]. However, the field of gain design for SEAs has not yet been explored. In this study, we propose a fourth order gain selection criterion, which uniquely defines both impedance and torque gains. This criterion only allows

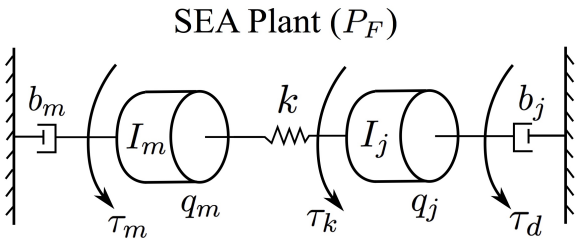


Fig. 2. **SEA Model Scheme.** $q_m, q_j$ represents motor and joint position, respectively. $k$ is the spring stiffness. $I_j, I_m$ is joint and motor inertia, respectively. $b_j, b_m$ are joint and motor damping coefficient, respectively. $I_m$ and $b_m$ are mapped to the joint coordinates by multiplying by the square of the gear reduction.

one variable to be determined by the designer, which is convenient for selecting controller gains.

In this study, we design a fourth order gain selection criterion to achieve critically-damped performance of series elastic actuators. Making multiple gains depend on a natural frequency reduces the degree of freedom for gain selection to one and this natural frequency represents the SEA impedance. To the best of our knowledge, this is the first time a critically-damped gain selection criterion has been proposed for SEAs. This criterion is supported by a detailed analysis of filtering and feedback delays and their influence in cascaded impedance control of SEAs. Finally, our theoretical results are validated through experimental implementations.

## II. Modeling of Series Elastic Actuators

In this section, we model a series elastic actuator that is subject to two nested control loops: an inner torque loop and an outer impedance loop. First, let us consider the SEA dynamics. As shown in Figure 2, the spring force $\tau_k$ is

$$\tau_k = k(q_m - q_j). \tag{1}$$

For the joint side, we assume external force $\tau_d = 0$ (i.e., spring torque is equal to load torque) and have

$$\tau_k = I_j \ddot{q}_j + b_j \dot{q}_j. \tag{2}$$

Note that this model only considers the effects of viscous joint friction; analysis of the effects of other types of friction is left for future work. The load plant $P_L(s)$ is then

$$P_L(s) = \frac{q_j(s)}{\tau_k(s)} = \frac{1}{I_j s^2 + b_j s}. \tag{3}$$

By Equations (1) and (2), we have the transfer function from motor position $q_m$ to joint position $q_j$.

$$\frac{q_j(s)}{q_m(s)} = \frac{k}{I_j s^2 + b_j s + k}. \tag{4}$$

Motor torque $\tau_m$ is represented as

$$\tau_m = I_m \ddot{q}_m + b_m \dot{q}_m + k(q_m - q_j). \tag{5}$$

Combining Equations (4) and (5) and defining $\Delta q = q_m - q_j$, we have the relationship between spring deflection and motor angle

$$r(s) = \frac{\Delta q(s)}{q_m(s)} = \frac{I_j s^2 + b_j s}{I_j s^2 + b_j s + k}. \tag{6}$$

Combining with Equation (1), spring force can be calculated

$$\tau_k(s) = k\Delta q(s) = k r(s) q_m(s). \tag{7}$$

Since the motor current $i_m$ and motor torque $\tau_m$ is related by

$$\frac{\tau_m(s)}{i_m(s)} = \beta = \eta N k_\tau, \tag{8}$$

with drivetrain efficiency $\eta$ (constant for simplicity, ignore dynamic model of drivetrain losses), gear speed reduction $N$ and motor torque constant $k_\tau$, the control plant $P_F(s)$ is

$$P_F(s) = \frac{\tau_k(s)}{i_m(s)} = \frac{\beta r(s) k}{I_m s^2 + b_m s + r(s)k}. \tag{9}$$

Then, from Figure 3, the closed-loop torque control plant $P_C$ is

$$P_C(s) = \frac{\tau_k(s)}{\tau_{des}(s)} = \frac{P_F(\beta^{-1} + C)}{1 + P_F C e^{-T_\tau s}}. \tag{10}$$

The torque feedback loop has a feedback delay $e^{-T_\tau s}$ and a PD compensator $C = K_\tau + B_\tau Q_{\tau d} s$, where $Q_{\tau d}$ is the filtering for torque derivative.

$$Q_{\tau d} = \frac{2\pi f_{\tau d}}{s + 2\pi f_{\tau d}}, \tag{11}$$

where $f_{\tau d}$ is the filter cut-off frequency. A feedforward term is designed to convert from desired torque $\tau_{des}$ to motor current $i_m$ as shown in Figure 3. By Equations (3) and (10), we have the following transfer function

$$\frac{q_j}{\tau_{des}} = P_L P_C = \frac{P_F(\beta^{-1} + C)}{(1 + P_F C e^{-T_\tau s})(I_j s^2 + b_j s)}. \tag{12}$$

The impedance feedback has the following form

$$\tau_{des}(s) = K_q(q_{des} - e^{-T_{qs} s} q_j) - B_q e^{-T_{qd} s} Q_{qd} s q_j, \tag{13}$$

where $e^{-T_{qs} s}$ and $e^{-T_{qd} s}$ represent the feedback delays in stiffness and damping loops, respectively. The first order low-pass filter $Q_{qd}$ for joint velocity has the same form as Equation (11) with a cut-off frequency $f_{qd}$. Using $P_L$ and $P_C$ in Equations (3) and (10), we can derive the system closed-loop transfer function $P_{CL}$ from $q_{des}$ to $q_j$,

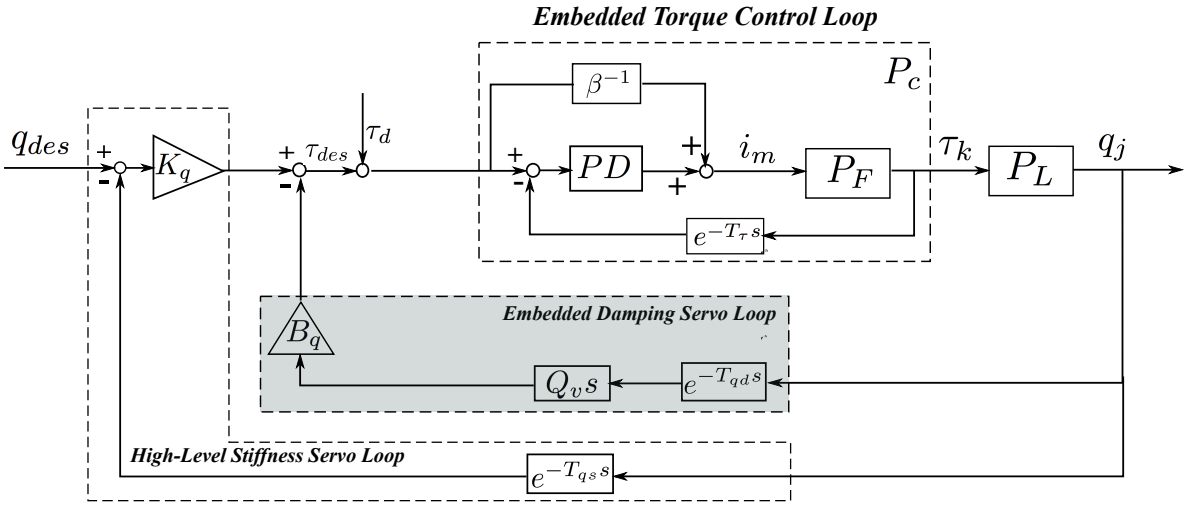


Fig. 3. **Joint-Level SEA Control Block Diagram.** The inner torque loop has proportional and derivative feedback and a feedforward loop with a mapping scaler $\beta^{-1}$. The outer impedance loop has stiffness and damping feedback. Our distributed controller proposes to embed the damping feedback at the low level while maintaining the stiffness loop for high-level tasks. Delays in each loop are labeled as $e^{-Ts}$. A first order low-pass filter is applied to both velocity and torque derivatives. The motor has a current input $i_m$. $\tau_k$ is the spring torque. $P_C$ represents the embedded torque control loop.

$$\begin{aligned} P_{CL}(s) &= \frac{q_j(s)}{q_{des}(s)} \\ &= \frac{K_q P_C P_L}{1 + P_C P_L (e^{-T_{qd}s} B_q Q_{qd} s + e^{-T_{qs}s} K_q)} \\ &= \frac{K_q(1 + \beta K_\tau + \beta B_\tau Q_{\tau d} s)}{\sum_{i=0}^{4} D_i s^i}, \end{aligned} \tag{14}$$

with coefficients

$$\begin{aligned} D_4 =& I_m I_j / k, \\ D_3 =& (I_j b_m + I_m b_j)/k + I_j \beta B_\tau Q_{\tau d} e^{-T_\tau s}, \\ D_2 =& I_j(1 + e^{-T_\tau s}\beta K_\tau) + I_m + b_j \beta B_\tau Q_{\tau d} e^{-T_\tau s} \\ &+ \beta B_\tau B_q e^{-T_{qd}s} Q_{qd} Q_{\tau d} + b_j b_m / k, \\ D_1 =& b_j(1 + e^{-T_\tau s}\beta K_\tau) + b_m + \beta B_\tau Q_{\tau d} K_q e^{-T_{qs}s} \\ &+ e^{-T_{qd}s}(1 + \beta K_\tau) B_q Q_{qd}, \\ D_0 =& e^{-T_{qs}s}(1 + \beta K_\tau) K_q. \end{aligned}$$

This transfer function is a sixth order system since the low pass filters $Q_{qd}$ and $Q_{\tau d}$ increase the order by two in total. An important issue to notice is that there is a zero in the numerator of Equation (14). This zero is caused by the torque derivative term. This induced zero will shorten the rise time but also cause an overshoot in step response. However, it does not influence system stability, which is determined by the characteristic polynomial in the denominator.

## III. Gain selection of series elastic actuator

Nested impedance and torque loops make controller gain design more challenging. This section proposes a method to design controller gains based on a critically-damped criterion.

### A. Critically-damped fourth order system gain criterion

For second order rigid actuators, impedance control gains [10] can be designed based on the well-known critically-damped criterion. For high order systems, there is no well-defined critically-damped criterion. However, high order systems can be often be represented as the product of first and second order systems. To achieve a critically-damped response for Equation (14), we represent this fourth order system by two multiplied second order systems [11]

$$(s^2 + 2\zeta_1\omega_1 s + \omega_1^2)(s^2 + 2\zeta_2\omega_2 s + \omega_2^2). \tag{15}$$

Note that we ignore feedback delay and filtering effect when designing controller gains. This allows the system to be a fourth order system instead of a higher one. Now we have four design parameters $\omega_1, \omega_2, \zeta_1, \zeta_2$, which are used to design four gains $K_q, B_q, K_\tau, B_\tau$. First, we set $\zeta_1 = \zeta_2 = 1$ in Equation (15) for a critically-damped purpose. Second, let us assume $\omega_2 = \omega_1$ for simplicity. We plan to study an optimal pole placement in future work. Now we can define the natural frequency $f_n$ of the fourth order system.

$$\omega_1 = \omega_2 \triangleq \omega_n = 2\pi f_n. \tag{16}$$

By comparing denominators of Equations (14) and (15), we have the following gain selection criterion equations.

$$\begin{aligned} &\frac{I_j b_m + I_m b_j + I_j \beta B_\tau k}{I_m I_j} = 4\omega_n, \\ &\frac{k(I_j(1 + \beta K_\tau) + I_m + \beta B_\tau (b_j + B_q)) + b_j b_m}{I_m I_j} = 6\omega_n^2, \\ &\frac{k(b_j + B_q)(1 + \beta K_\tau) + k(b_m + \beta B_\tau K_q)}{I_m I_j} = 4\omega_n^3, \\ &\frac{(1 + \beta K_\tau) k K_q}{I_m I_j} = \omega_n^4. \end{aligned} \tag{17}$$

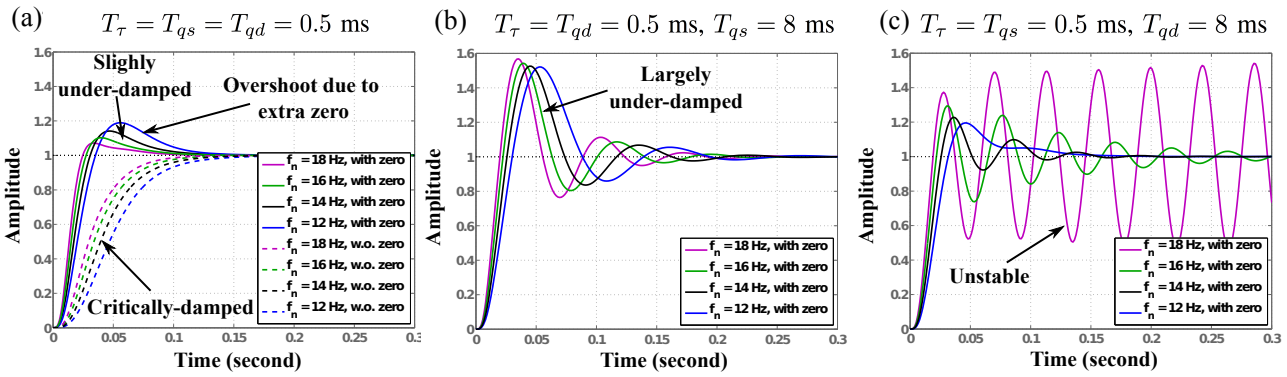


Fig. 4. **SEA Step Response with Effects from Feedback Delays and An Extra Zero.** These subfigures demonstrate that large impedance feedback delays deteriorate step response performance. Comparing subfigures (b) and (c), we observe that system stability is more sensitive to damping feedback delays than its stiffness counterpart. Note that, in subfigure (a), the larger $f_n$ is, the larger the overshoot, which seems counterintuitive. However, if observed closely, the solid magenta line with the largest $f_n$ already shows distortion and its phase margin value is $36.4^\circ$, smaller than other three cases. Also, to analyze the effect of zero in Equation (14), we simulate step responses without this zero, shown in dashed lines of subfigure (a). By comparison, we can observe this extra zero induces an overshoot.

TABLE I
CRITICALLY-DAMPED GAIN SELECTION RULE

| Frequency (Hz) | Impedance Gains (Nm/rad, Nms/rad) | Torque Gains (A/Nm, As/Nm) | Phase Margin |
|---|---|---|---|
| $f_n = 12$ | $K_q = 65$<br>$B_q = 0.46$ | $K_\tau = 1.18$<br>$B_\tau = 0.057$ | $49.1^\circ$ |
| $f_n = 14$ | $K_q = 83$<br>$B_q = 0.76$ | $K_\tau = 1.80$<br>$B_\tau = 0.067$ | $47.0^\circ$ |
| $f_n = 16$ | $K_q = 103$<br>$B_q = 1.02$ | $K_\tau = 2.56$<br>$B_\tau = 0.077$ | $43.6^\circ$ |
| $f_n = 18$ | $K_q = 124$<br>$B_q = 1.26$ | $K_\tau = 3.45$<br>$B_\tau = 0.087$ | $39.9^\circ$ |
| $f_n = 20$ | $K_q = 148$<br>$B_q = 1.49$ | $K_\tau = 4.48$<br>$B_\tau = 0.097$ | $36.4^\circ$ |

These nonlinear equations can be solved using Matlab's `fsolve` function. Table I shows five natural frequency cases. As $f_n$ increases, all four gains increase simultaneously, which is consistent with our intuition that increasing torque (or impedance) gains will increase system torque (or impedance) bandwidth. Note that, when calculating phase margins, we incorporate filters $f_{vd} = 50$ Hz, $f_{\tau d} = 100$ Hz and feedback delays $T_\tau = T_{qs} = T_{qd} = 0.5$ ms.

Now let us consider how impedance feedback loop delays affect the SEA step response. Since torque feedback is regarded as the inner loop, it always has the smallest delay, $T_\tau = 0.5$ ms in our case, than the other two impedance loops. As observed in Figure 4, system stability is more sensitive to damping delays than stiffness delays. The case with $T_{\tau d} = T_{qd} = 0.5$ ms, $T_{qs} = 8$ ms is analogous to our proposed distributed control architecture in [10].

### *B. Trade-off between impedance control and torque control*

The motivation first came from gain tuning work on our bipedal robot, which uses a similar cascaded control architecture in Figure 3. We observed that, when torque gains increased or when impedance gains decreased, the robot's motions became less stable. To validate this phenomenon, we made simulations where a gain scale, $GS$, was used between adjusted gains $(K_{i_a}, B_{i_a})$ and nominal gains $(K_{i_n}, B_{i_n})$, $i \in \{\tau, q\}$. Adjusted gains are the real gains used in the simulations while nominal gains are the gains determined from the fourth order system gain selection criterion. For instance, we choose the gain set of $f_n = 14$ Hz in Table I as nominal gains $(K_{i_n}, B_{i_n}), i \in \{\tau, q\}$. Adjusted gains $(K_{i_a}, B_{i_a}), i \in \{\tau, q\}$ are obtained by a gain scale below

$$GS = \frac{K_{\tau_a}}{K_{\tau_n}} = \frac{K_{q_n}}{K_{q_a}}.$$

Similarly, the damping gains are related to GS by

$$GS = \frac{B_{\tau_a}}{B_{\tau_n}} = \frac{B_{q_n}}{B_{q_a}},$$

which guarantees multiplication of cascaded proportional (or damping) torque and impedance gains are the same for both normal and adjusted cases, i.e.,

$$\begin{aligned} K_{\tau_a} \cdot K_{q_a} &= K_{\tau_n} \cdot K_{q_n}, \\ B_{\tau_a} \cdot B_{q_a} &= B_{\tau_n} \cdot B_{q_n}. \end{aligned} \tag{18}$$

A similar observation is obtained in [12] where increasing the inner loop controller bandwidth reduces the stable range of impedance parameters. A trade-off exists between a high torque bandwidth to provide accurate torque tracking and a low torque bandwidth to increase the stable range of impedance gains. However, the experimental validation in [12] is not completely persuasive because impedance gains are not reduced when torque gains are increased. This means that the multiplication of two cascaded gains increases. In this case, system stability obviously decreases. Instead, our study assumes a constant gain multiplication and then focuses on the trade-off between torque and impedance gains. Subfigure (a) in Figure 5 represents the nominal case with $GS = 1$. As observed, when torque gains increase and impedance gains

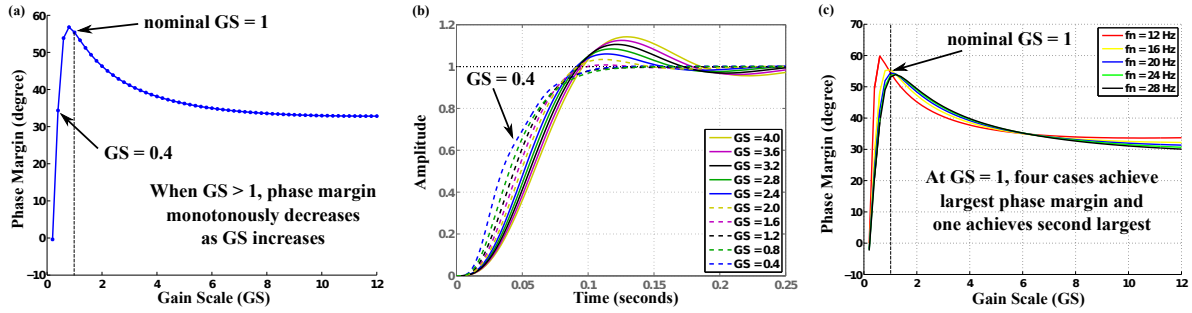


Fig. 5. **Different Gain Scales between Impedance and Torque Gains.** Subfigure (a) shows that our critically-damped gain selection is a sub-optimal solution since its phase margin is the second best. As subfigure (b) shows, increasing GS will slow down the rise time and cause larger overshoot. This means larger GS deteriorates system stability. However, decreasing GS may decrease phase margin as well. $GS = 0.4$ has a phase margin around $34^\circ$ in subfigure (a) and its step response has a distortion in subfigure (b), although behaving more over-damped. Subfigure (c) samples a range of natural frequencies for the nominal gains and all of them demonstrate similar results. Filtering and delays are ignored to focus on effects of different gain scales.

decrease (i.e., $GS > 1$), system shows larger oscillatory step response in subfigure (b) and its phase margin becomes smaller in subfigure (a). This result validates our observation that using larger torque gains deteriorates SEA phase margin based stability. Note that, when $GS \neq 1$, there is no well-defined $f_n$, which is only proposed in the case of critically-damped gains, i.e., $GS = 1$. Indeed, in our implementations we only use the critically-damped gains due to their resulting optimal behaviors. The purpose of considering $GS \neq 1$ is to study the trade-off phenomenon.

Impedance control is suitable for dynamic interaction between robots and their environment [6]. Since legged robots inevitably have contact impact, it is necessary to study how SEA impedance behaves within different frequency ranges based on the gain selection criterion proposed above.

## IV. SEA IMPEDANCE ANALYSIS WITH FILTERING AND FEEDBACK DELAY EFFECTS

In this section, we derive the SEA impedance transfer function based on the control block diagram in Figure 3 and analyze different frequency range characteristics with considerations of filtering and delays. Recall that the higher the natural frequency $f_n$, the higher the SEA impedance. Let us first derive the SEA impedance transfer function.

### A. SEA impedance transfer function

To study the impedance of SEA dynamics, we choose joint velocity $q_j$ as input and joint torque $\tau_j$ as output. Given zero desired joint position $q_{des}$, the impedance transfer function $Z(s) = \tau_j(s)/(-sq_j(s))$ is formulated as follows.

$$Z(s) = \frac{\tau_j(s)}{-sq_j(s)} = \frac{\sum_{i=0}^{4} N_{zi} s^i}{\sum_{i=0}^{5} D_{zi} s^i}, \tag{19}$$

with numerator coefficients

$$\begin{aligned}
N_{z4} =& I_m T_{f\tau} T_{fv} \beta k, \\
N_{z3} =& \beta k (I_m (T_{f\tau} + T_{fv}) + T_{f\tau} T_{fv} b_m), \\
N_{z2} =& I_m \beta k + \beta k b_m (T_{f\tau} + T_{fv}) + k k_\tau \\
& (T_{f\tau} + \beta (B_\tau + K_\tau T_{f\tau}))(B_q e^{-T_{qd} s} + K_q T_{fv} e^{-T_{qs} s}), \\
N_{z1} =& b_m \beta k + B_q k k_\tau (1 + K_\tau \beta) e^{-T_{qd} s} + K_q k k_\tau \\
& (T_{fv} + T_{f\tau} + \beta (B_\tau + K_\tau (T_{f\tau} + T_{fv}))) e^{-T_{qs} s}, \\
N_{z0} =& K_q k k_\tau e^{-T_{qs} s} (1 + K_\tau \beta),
\end{aligned}$$

and the denominator coefficients

$$\begin{aligned}
D_{z5} =& I_m T_{f\tau} T_{fv} \beta, \\
D_{z4} =& I_m \beta (T_{fv} + T_{f\tau}) + T_{fv} T_{f\tau} \beta b_m, \\
D_{z3} =& \beta I_m + \beta b_m (T_{f\tau} + T_{fv}) + T_{fv} k \beta (T_{f\tau} \\
& + k_\tau (B_\tau + K_\tau T_{f\tau}) e^{-T_\tau s}), \\
D_{z2} =& \beta (b_m + T_{f\tau} k + k k_\tau (B_\tau + K_\tau T_{f\tau}) e^{-T_\tau s}) \\
& + T_{fv} \beta k (1 + K_\tau k_\tau e^{-T_\tau s}), \\
D_{z1} =& \beta k (1 + K_\tau k_\tau e^{-T_\tau s}), D_{z0} = 0.
\end{aligned}$$

Note that, joint inertia $I_j$ and damping $b_j$ at the load side are not included in $Z(s)$ since they are regarded as the interacted environment. When analyzing this SEA impedance, we incorporate effects of filtering and feedback delays. As far as we know, results in literature are still missing that analyze the filtering and delay effects on SEA impedance of a cascaded control structure with nested inner PD torque control and outer impedance control. Results in [3] analyzes another typical cascaded control architecture with a proportional-integral torque loop and an inner-most motor velocity loop. However, they only consider sampling rate delay instead of large delays such as communication bus delays. Also, they neglect integral gains during SEA impedance analysis for simplicity. Instead, our study uses the exact transfer function in Equation (19) without any approximations.

### B. Effects of filtering and feedback delays on SEA impedance

SEA impedance results are shown in Figure 6. Four cases are studied with or without velocity filtering and feedback delays:

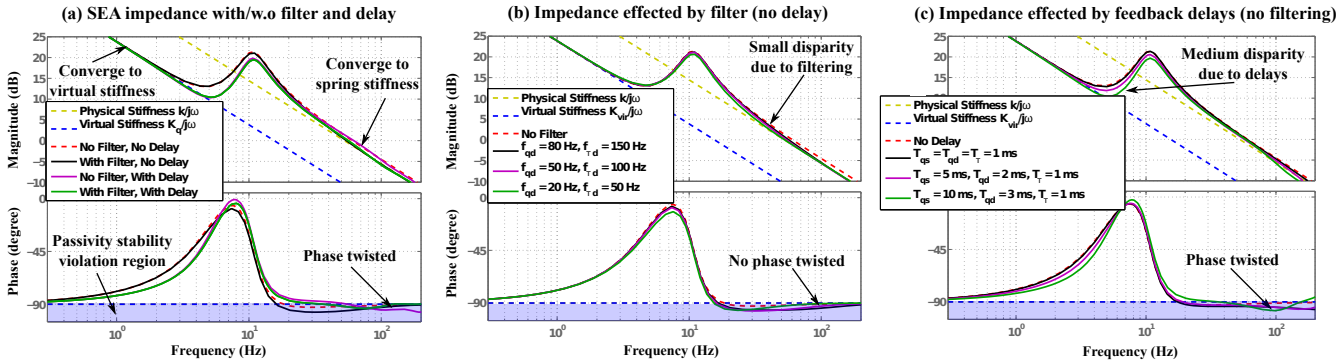


Fig. 6. **SEA Impedance Effected by Filtering and Feedback Delays.** In subfigure (a), the yellow and blue dashed lines represent impedance of physical spring stiffness $k$ and a virtual stiffness gain, respectively. The red dashed line is the ideal SEA impedance without filtering and delay. At low frequencies, SEA impedance approaches the virtual stiffness, similar to that in [3]. At medium and high frequencies, it converges to another impedance asymptote. Subfigure (b) analyzes the effect of the filter while subfigure (c) analyzes the effect of feedback delays. Similarly, the sensitivity to different feedback delays can be analyzed but is not discussed here due to space limitations. A natural frequency of $f_n = 30$ Hz is used for all simulations in this figure with $K_q = 293.6Nm/rad, B_q = 2.49Nms/rad, K_\tau = 11.71A/Nm, B_\tau = 0.146As/Nm$.

(I) $Z_i(j\omega)$, ideal impedance without filtering and delays; (II) $Z_f(j\omega)$, impedance with filtering only; (III) $Z_d(j\omega)$, impedance with delays only; (IV) $Z_{fd}(j\omega)$, impedance with both filtering and delays. At low frequencies, it is observed that SEA impedance approaches a virtual stiffness in any of the four cases above (if feedback delays exist, $e^{-T_{qs}j\omega} \to 1, e^{-T_\tau j\omega} \to 1$ as $\omega \to 0$)

$$\lim_{\omega\to 0} Z_c(j\omega) = \lim_{\omega\to 0} \frac{N_{z0}}{j\omega \cdot D_{z1}} = \frac{K_q k_\tau(\beta^{-1} + K_\tau)}{j\omega \cdot (1 + K_\tau k_\tau)}, \quad (20)$$

where $c \in \{i, f, d, fd\}$. We keep $j\omega$ in final expression for indicating the existence of a $-20$ dB/dec asymptote. The low frequency impedance $Z_c(j\omega)$ behaves like a pure virtual stiffness impedance $K_q/j\omega$ with a scaling $k_\tau(\beta^{-1} + K_\tau)/(1 + K_\tau k_\tau)$. This scaling exists for any PD-type cascaded impedance controller. However, $k_\tau\beta^{-1}$ is normally very small. When $k_\tau K_\tau$ is larger, $Z_c(j\omega)$ approaches to $K_q/j\omega$, more behaving like a pure spring $K_q/j\omega$.

In the case of high frequencies, the impedance magnitude approaches or twists around an asymptote, depending on specific cases. First, let us consider the ideal case (I), i.e., without filtering and delays. We have $D_{z5} = D_{z4} = 0$.

$$\lim_{\omega\to+\infty} Z_i(j\omega) = \lim_{\omega\to+\infty} \frac{N_{z2}}{j\omega \cdot D_{z3}} = \frac{k(I_m + k_\tau B_\tau B_q)}{j\omega \cdot I_m} \quad (21)$$

which is a constant stiffness impedance but differs from the pure spring stiffness. Figure 6 (b)-(c) shows that the red dashed line represents an ideal SEA impedance and it approaches another asymptote at high frequencies.

Second, let us consider case (III) with delay only, i.e. $T_{fv} = T_{f\tau} = 0$. We also have $D_{z5} = D_{z4} = 0$.

$$\lim_{\omega\to+\infty} Z_d(j\omega) = \lim_{\omega\to+\infty} \frac{N_{z2}}{j\omega \cdot D_{z3}} = \frac{k(I_m + k_\tau B_\tau B_q e^{-T_{qd}s})}{j\omega \cdot I_m} \quad (22)$$

Since the complex number $e^{-T_{qd}s}$ periodically rotates along the unit circle, SEA impedance twists around the impedance of pure spring stiffness at high frequencies. This can be checked at the high frequency range of both magnitude and phase plots in Figure 6 (c).

Third, in Case (II) with filtering only, i.e. $T_{qs} = T_{qd} = T_\tau = 0$.

$$\lim_{\omega\to+\infty} Z_f(j\omega) = \frac{N_{z4}}{j\omega D_{z5}} = \frac{k}{j\omega} \quad (23)$$

which has a $-20$ dB/dec asymptote as shown in Figure 6 (b). No curve twist shows up since the limit value is a constant. By comparing Figure 6 (b) and (c), it is obvious to notice that delay has significantly large effect on the deviation from ideal SEA impedance.

Practical factors from filtering and delay indeed influence practical impedance. Based on the passivity stability criterion [7], [3], [13], the phase value should remain within $-90°$ and $90°$ (the blue region). As we see, the SEA impedance has phase value smaller than $-90°$, which violates the passivity criterion. However, a non-passive system does not mean the system is unstable. For instance, all four cases in Figure 6 (a) violate the passivity condition, but two cases without filtering have phase margins larger than $54°$ while two cases with filtering have phase margins larger than $16°$. Moreover, filtering and delays make the magnitude and phase curve twisted at high frequency range. These effects are commonly ignored in existing literatures but they certainly play important roles in real implementations.

### C. Effects of load inertia on SEA impedance

In this subsection, we study how load inertia affects SEA impedance. In practice, the port of interaction with the environment contains a load inertia. Thus, a load inertia $I_j s$ is added into Equation (19), i.e., $Z_l(j\omega) = Z(j\omega) + I_j s$. Then, SEA impedance behaves like a spring-mass instead of a pure spring at high frequencies. Specifically, it is dominated

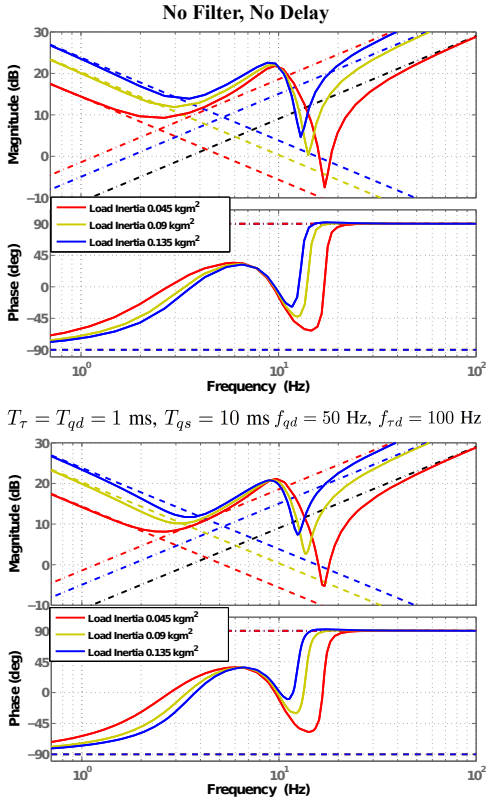


Fig. 7. **Effects of Load Inertia on SEA Impedance.** This figure shows three different load scenarios. At high frequencies, SEA impedance approaches the load inertia impedance $I_j \cdot s$. Filtering and delays provides very limited effect since two figures perform very similar.

by the inertia in Figure 7. Four different loads are simulated. For Equation (19). $Z(j\omega) \to 0$ as $\omega \to +\infty$. Thus we have

$$\lim_{\omega \to +\infty} Z_l(j\omega) = \lim_{\omega \to +\infty} (Z(j\omega) + I_j \cdot j\omega) = I_j \cdot j\omega$$

Thus, $I_j \cdot j\omega$ is the asymptote at high frequencies in Figure 7 when an inertia is attached to the load side. Thus, the SEA impedance will exhibit the high impedance caused by the load inertia at high frequencies.

## V. Experimental Validation

In this section, we use our UT-SEA testbed [14] to validate theoretical and simulation results. All of the controller gains are designed based on the gain selection criterion. In Figure 8, we observe that the larger the natural frequency is, the higher the bandwidth of the closed-loop system is. Simulations and experiments match each other with the exception of a slight discrepancy at high frequency range. Refer back to Table I for the normalized values of virtual stiffness and damping used in this test. With respect to the trade-off between torque gains and impedance gains, Figure 9 demonstrates that when $GS > 1$, system step response exhibits larger overshoot and slower rise time. This validates our conjecture that increasing torque gains while decreasing impedance gains deteriorates

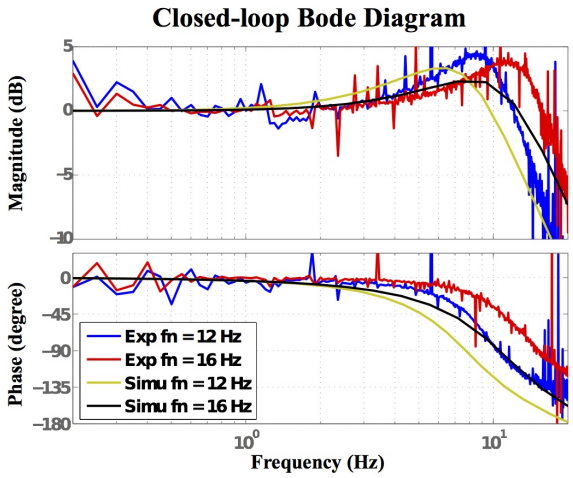


Fig. 8. **Bode Diagrams with Different Natural Frequencies** $f_n$. This figure shows that increasing $f_n$ increases closed-loop bandwidth. At low frequencies, experiments match simulations quite well. At frequencies around resonant frequency, experiments show a larger resonant peak and a slightly larger bandwidth than simulations.

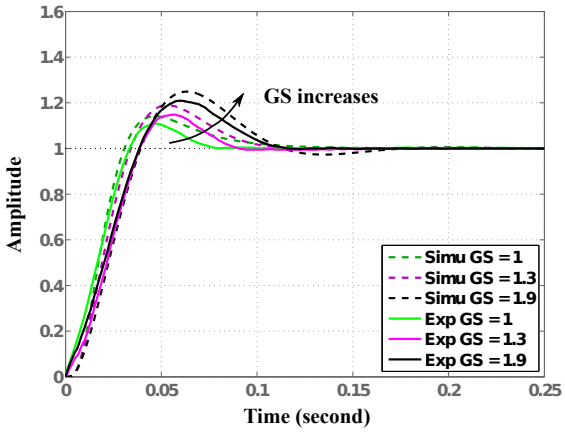


Fig. 9. **Comparison of Simulations and Experiments with Different Gain Scales** Experimental data matches simulations with a small discrepancy on the overshoot. This discrepancy probably comes from unmodelled dynamics and Coulomb friction. It validates that increasing torque gains and decreasing impedance gains deteriorate system stability.

system stability. As to the discrepancy in these two tests, one main factor is that our SEA uses a timing belt, which induces inevitable elasticity. However, it is difficult to model its elasticity and incorporate it into controller design.

For dynamic legged locomotion [15], torque tracking under impact dynamics is important for stable and agile walking. By implementing an impulse test, we show how accurately our controller reacts to the varied desired torques under external impulse disturbances. As shown in Figure 10, when a ball free falls from 20 cm height and hits the arm with an impulse force, the SEA actuator settles down promptly and recovers after approximately 0.3 seconds. Joint torque tracking is quite accurate with only minor distortion around peak values.

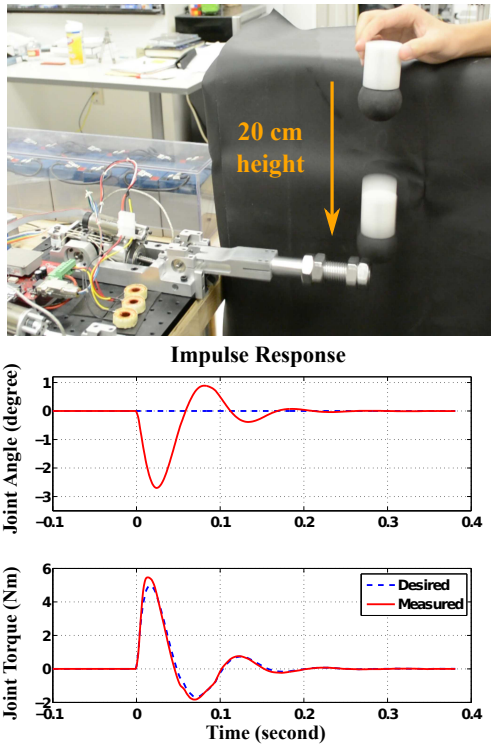


Fig. 10. **Impulse Response of UT-SEA**. A ball is dropped from a height (20 cm) and exerts an impulse force on the arm end-effector. The maximum angle deviation is around 2.5 degrees. The arm recovers its initial position within 0.3 seconds. Joint torque exhibits accurate torque tracking.

## VI. Conclusion and Discussions

This study proposed a controller gain design method for the fourth order SEA system and analyzed SEA impedance at different frequency ranges. By considering the trade-off between torque gains and impedance gains, we demonstrate our critically-damped gain selection is optimal, and increasing torque gains while decreasing impedance gains will deteriorate system stability. Meanwhile, filtering and feedback delays are incorporated into our framework. Additionally, our method is not limited by the conservative passivity criterion.

Our on-going work focuses on the following aspects: (I) Systematically quantify the effects of filtering and delays on closed-loop stability and SEA impedance. Additionally, we are exploring the fundamental causes of the phase margin sensitivity discrepancy analogous to that in [10]; (II) Since critically-damped gain selection achieves near-optimal stability in terms of system phase margin, we will explore its fundamental reasons; (III) Study a novel stability criterion which removes conservative assumptions for passivity condition. A good reference is the stability Routh-Hurwitz criterion proposed in [16]; (IV) Implement the fourth order gain selection criterion on our Hume bipedal robot. The gain selection criterion proposed here will serve as a foundation of our long term goal of implementing Cartesian impedance control on dynamic legged locomotion on rough terrain [15].

## References


[1] G. A. Pratt, P. Willisson, C. Bolton, and A. Hofman, "Late motor processing in low-impedance robots: Impedance control of series-elastic actuators," in *American Control Conference, 2004. Proceedings of the 2004*, vol. 4. IEEE, 2004, pp. 3245–3251.

[2] M. Hutter, C. D. Remy, M. A. Hoepflinger, and R. Siegwart, "Efficient and versatile locomotion with highly compliant legs," *Mechatronics, IEEE/ASME Transactions on*, vol. 18, no. 2, pp. 449–458, 2013.

[3] H. Vallery, J. Veneman, E. Van Asseldonk, R. Ekkelenkamp, M. Buss, and H. Van Der Kooij, "Compliant actuation of rehabilitation robots," *Robotics & Automation Magazine, IEEE*, vol. 15, no. 3, pp. 60–69, 2008.

[4] N. L. Tagliamonte, D. Accoto, and E. Guglielmelli, "Rendering viscoelasticity with series elastic actuators using cascade control," in *Robotics and Automation (ICRA), 2014 IEEE International Conference on*. IEEE, 2014.

[5] M. Mosadeghzad, G. A. Medrano-Cerda, J. A. Saglia, N. G. Tsagarakis, and D. G. Caldwell, "Comparison of various active impedance control approaches, modeling, implementation, passivity, stability and trade-offs," in *Advanced Intelligent Mechatronics (AIM), 2012 IEEE/ASME International Conference on*. IEEE, 2012, pp. 342–348.

[6] N. Hogan, "Impedance control: An approach to manipulation: Part iiimplementation," *Journal of dynamic systems, measurement, and control*, vol. 107, no. 1, pp. 8–16, 1985.

[7] J. E. Colgate and J. M. Brown, "Factors affecting the z-width of a haptic display," in *Robotics and Automation, 1994. Proceedings., 1994 IEEE International Conference on*. IEEE, 1994, pp. 3205–3210.

[8] T. Boaventura, G. A. Medrano-Cerda, C. Semini, J. Buchli, and D. G. Caldwell, "Stability and performance of the compliance controller of the quadruped robot hyq," in *Intelligent Robots and Systems (IROS), 2013 IEEE/RSJ International Conference on*. IEEE, 2013, pp. 1458–1464.

[9] K. Kong, J. Bae, and M. Tomizuka, "Control of rotary series elastic actuator for ideal force-mode actuation in human–robot interaction applications," *Mechatronics, IEEE/ASME Transactions on*, vol. 14, no. 1, pp. 105–118, 2009.

[10] Y. Zhao, N. Paine, and L. Sentis, "Sensitivity comparison to loop latencies between damping versus stiffness feedback control action in distributed controllers," in *ASME 2014 Dynamic Systems and Control Conference*. American Society of Mechanical Engineers, 2014.

[11] F. Petit and A. Albu-Schaffer, "State feedback damping control for a multi dof variable stiffness robot arm," in *Robotics and Automation (ICRA), 2011 IEEE International Conference on*. IEEE, 2011, pp. 5561–5567.

[12] M. Focchi, G. A. Medrano-Cerda, T. Boaventura, M. Frigerio, C. Semini, J. Buchli, and D. G. Caldwell, "Robot impedance control and passivity analysis with inner torque and velocity feedback loops," *arXiv preprint arXiv:1406.4047*, 2014.

[13] C. Ott, A. Kugi, and G. Hirzinger, "On the passivity-based impedance control of flexible joint robots," *Robotics, IEEE Transactions on*, vol. 24, no. 2, pp. 416–429, 2008.

[14] N. Paine, S. Oh, and L. Sentis, "Design and control considerations for high-performance series elastic actuators," *IEEE/ASME Transactions on Mechatronics*, vol. 19, no. 3, pp. 1080–1091, 2014.

[15] Y. Zhao and L. Sentis, "A three dimensional foot placement planner for locomotion in very rough terrains," in *Humanoid Robots (Humanoids), 2012 12th IEEE-RAS International Conference on*. IEEE, 2012.

[16] T. Hulin, R. G. Camarero, and A. Albu-Schaffer, "Optimal control for haptic rendering: Fast energy dissipation and minimum overshoot," in *Intelligent Robots and Systems (IROS), 2013 IEEE/RSJ International Conference on*. IEEE, 2013, pp. 4505–4511.